Liquid−Liquid Phase Behavior of Solutions of 1-Octyl- and 1-Decyl-3-methylimidazolium Bis(trifluoromethylsulfonyl)imide ($C_{8,10}$mimNTf_2) in *n*-Alkyl Alcohols†

Vlad R. Vale,‡ Bernd Rathke,*,‡ Stefan Will,‡ and W. Schröer§

Universität Bremen, Technische Thermodynamik, Badgasteiner Str. 1, 28359 Bremen, Germany, and Universität Bremen, FB2, Institut für Anorganische und Physikalische Chemie, Leobener Str. NWII, 28359 Bremen, Germany

Systematic measurements of liquid−liquid phase diagrams of binary mixtures of the ionic liquids 1-octyl-3-methylimidazolium bis(trifluoromethylsulfonyl)imide (C_8mimNTf_2) and 1-decyl-3-methylimidazolium bis(trifluoromethylsulfonyl)imide (C_{10}mimNTf_2) with *n*-alkyl alcohols (1-octanol, 1-nonanol, 1-decanol, 1-undecanol, 1-dodecanol, 1-tetradecanol, 1-hexadecanol, 1-octadecanol, and 1-eicosanol) were performed. The phase diagrams were obtained at atmospheric pressure in the temperature range (283 to 423) K applying the cloud-point method on a set of samples. With the assumption of Ising criticality, analysis of the shapes of the phase diagrams yielded data on the critical points and the parameters characterizing the width and the asymmetry of the coexistence curves.

Introduction

The melting temperatures of typical inorganic salts are above 1000 K. In contrast, certain organic salts, termed ionic liquids (ILs),[1] have melting temperatures below 373 K; some ILs become liquids at temperatures as low as 200 K.[2] The remarkably low melting points originate from the chemical structure of the ILs, which are composed of an inorganic or organic anion and a rather large, asymmetrical organic cation. Because of the presence of free charges with Coulomb interactions and long organic side chains, ILs have many special properties.[3−5] The strong Coulomb interactions cause the vapor pressure to be so low that it can hardly be measured,[6] and the boiling temperature is estimated to be above 1300 K,[7] although this is not observable because the chemical stability of ILs ceases near 600 K.[8,9] Nevertheless, it can be said that the liquid range of up to 400 K is remarkably large[10] in comparison with nonionic solvents. Chemical modification of the ions enables variation of the solvent properties, so some ILs are miscible with water[11−13] while others are soluble in hydrocarbons.[14−17] Because of those properties, there is a high interest in applying ILs in chemical engineering, e.g., as solvents in synthesis and separation techniques.[18,19] Phase diagrams of liquid−liquid equilibria are important basic data for applications such as extractions. Although quite a few data for binary mixtures with ILs of different anions have recently been reported,[11−32] systematic studies are still required in order to provide information for assessing the relations between the phase diagrams of the solutions of ILs and the chemical structures of the components by empirical analysis and theoretical methods. This work aims to contribute to this program. Mixtures with alcohols are of particular interest because the influence of the chain length of the alcohols on the phase diagrams can be studied in detail. In principle, such an investigation can cover the whole range from water to hydrocarbons and from highly polar to nonpolar solvents.[12,14,32] ILs with the anion bis(trifluoromethylsulfonyl)imide (NTf_2) are presently of high interest because this anion is rather hydrophobic, making the ILs soluble in nonpolar solvents. Furthermore, it is stable with respect to hydrolysis, in contrast to ILs with the anions BF_4^- and PF_6^-,[33] whose solutions have been investigated extensively.[11−13,23−26] In this work, we have extended previous investigations[21,22,25,26,29,31] of mixtures of ILs containing the NTf_2 anion and imidazolium cations with *n*-alkyl alcohols (C_nOH) of short chain length to include alcohols with longer chain lengths ($n = 8$ to 20) and to consider ILs with slightly longer side chains ($x = 8$, 10) on the methylimidazolium ($C_x$mim) cation. Because of the increasing tendency for the formation of liquid-crystalline domains of the methylimidazolium salts with longer side chains ($x > 10$), the present study was limited to systems with $x \leq 10$, which show only increasing segregation but no formation of liquid crystals (e.g., see ref 34). Figure 1 gives the chemical structure of $C_x$mimNTf_2. In total, we report data for 17 phase diagrams.

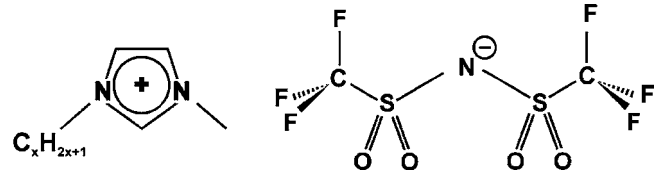

Figure 1. Structures of the ionic liquids 1-octyl- and 1-decyl-3-methylimidazolium bis(trifluoromethylsulfonyl)imide, abbreviated as C_8mimNTf_2 and C_{10}mimNTf_2, respectively.

Experimental Section

Materials. The *n*-alkyl alcohols 1-octanol ($C_8H_{18}O$, CAS no. 11-87-5, ≥ 99 %), 1-nonanol ($C_9H_{20}O$, CAS no. 143-08-8, ≥ 98 %), 1-decanol ($C_{10}H_{22}O$, CAS no. 112-30-1, ≥

† Part of the "Josef M. G. Barthel Festschrift".

* To whom correspondence should be addressed. Tel.: +49 421 218 3334. Fax: +49 421 218 7555. E-mail: rathke@uni-bremen.de.
‡ Technische Thermodynamik.
§ Institut für Anorganische und Physikalische Chemie.

10.1021/je900988a
Published on Web 03/11/2010

99 %), 1-undecanol ($C_{11}H_{24}O$, CAS no. 112-42-5, ≥ 98 %), 1-dodecanol ($C_{12}H_{26}O$, CAS no. 112-53-8, ≥ 99 %), 1-tetradecanol ($C_{14}H_{30}O$, CAS no. 112-72-1, ≥ 98 %), 1-hexadecanol ($C_{16}H_{34}O$, CAS no. 36653-82-4, ≥ 95 %), 1-octadecanol ($C_{18}H_{38}O$, CAS no. 112-92-5, > 99 %), and 1-eicosanol ($C_{20}H_{42}O$, CAS no. 629-96-9, ≥ 96 %) were purchased from Merck KGaA (Darmstadt, Germany) with the maximum available purity and used without further purification. The ionic liquids 1-octyl-3-methylimidazolium bis(trifluoromethylsulfonyl)imide ($C_{14}H_{19}F_6N_3O_4S_2$, C_8mimNTf$_2$, CAS no. 178631-04-4, > 98 %, 70 ppm water) and 1-decyl-3-methylimidazolium bis(trifluoromethylsulfonyl)imide ($C_{16}H_{23}F_6N_3O_4S_2$, C_{10}mimNTf$_2$, CAS no. 433337-23-6, > 98 %; 30 ppm water) were purchased from IoLiTec (Ionic Liquids Technologies GmbH, Denzlingen, Germany) and were degassed and dried before sample preparation. In order to remove the water and any volatiles, the IL $C_x$mimNTf$_2$ was added to a 100 mL round-bottom flask (Schott Duran glass) under an inert argon atmosphere inside a glovebag (Atmos-Bag, Sigma-Aldrich) and dried under continuous stirring at a temperature of 318 K for about 12 h under a vacuum of $2 \cdot 10^{-5}$ bar. The sample was frequently separated from the vacuum line to monitor the drying process by weighing the sample. We checked the mass loss of a typical 40 g sample of IL after the process of drying and found that the detectable loss of mass was less than 10^{-3} g within a period of 2 h.

Sample Preparation. The phase diagrams were determined using the synthetic method. The mixtures of IL and alcohol were prepared in culture tubes (glass type: Schott Duran) with heat-resistant screw caps made of PBT with a seal made of PTFE-coated silicon under a protective gas atmosphere (argon) to avoid contact with air and humidity. A minimum of 10 samples with mole fractions between 0.02 and 0.45 were prepared for each binary mixture by weighing each component directly into the sample tubes; the typical size of a sample was 2 g. The composition was determined gravimetrically with an accuracy of 10^{-3} g, resulting in an overall uncertainty in the mole fraction of $\Delta x_{IL} = \pm 10^{-3}$.

Cloud-Point Detection. The transition temperatures defining the liquid−liquid phase diagrams of the IL + alcohol binary mixtures were determined by the cloud-point method. For measurements in the lower-temperature region, T = (290 to 340) K, a transparent water bath was used. The temperature was controlled by a thermostat (Haake DC 30, Thermo, Karlsruhe, Germany), and the temperature stability was ± 0.02 K. In the higher-temperature range, T = (340 to 430) K, the measurements were carried out in a silicon oil bath with a temperature stability better than ± 0.05 K (Lauda, Proline RP845/PV15). In both cases, temperatures were measured using a Pt-100 sensor connected to a high-precision resistance thermometer (Kelvimat 4323, Burster, Gernsbach, Germany) with an uncertainty of ± 0.05 K.

The cloud-point temperatures were determined by systematically constraining the temperature range of observation and appropriately reducting the temperature steps in the temperature range considered. At first, the prepared samples with known mole fraction were heated to about 5 K above the critical temperature for about 20 min and homogenized using either a Vortex mixer or a magnetic stirrer. The temperature was then decreased in steps of typically (0.5 to 5) K until the two-phase region was reached. The onset of the phase transition was visually observed. The temperature was increased again until the sample reached the one-phase region. These steps were repeated until the temperature interval in which the cloud point temperature was observed within a time of up to 10 min reached 0.1 K near the critical point and (0.1 to 0.3) K near the edges of the phase diagrams. The cloud points and their repeatability were determined by frequent repetition of this procedure, starting from the one-phase region at different initial temperatures and reducing the temperature in steps of 0.05 K at the top of the phase diagrams and steps of (0.2 to 1) K at the edges. As first-order phase transitions, especially at the edges of the phase diagram, occur only under highly supersaturated conditions and as the onset of demixing depends on the speed of penetration into the metastable region, the cooling rate was also varied between (0.05 and 1) $K \cdot min^{-1}$. This procedure minimized the uncertainties arising from the subjectivity of the observer, the appearance of metastable states, and kinetic effects. Thus, the uncertainties δT of the cloud-point temperatures T_{cloud} given in Table 1 were determined by the accuracy of the T measurements and the repeatability of the observed transition temperatures: the lower limit of the uncertainty of T_{cloud} is given by the accuracy of the T measurement, while larger values of the repeatability of T_{cloud} result in higher uncertainties of this value. A cross-check using different batches of the substances used in this study showed no significant variations, yet uncontrollable traces of other impurities might have affected the results in a systematic way. This, together with the statistical error, resulted in a slight scatter of the cloud-point temperatures, which could be estimated from the standard deviation of the fits from the experimental data.

Results and Discussion

Experimental Results. The results of the phase diagram measurements are listed in Tables 1 and 2. Table 1 gives the mass fractions, mole fractions, cloud-point temperatures, and uncertainties of the measurements for the solutions of C_8mimNTf$_2$, and Table 2 provides the same data for the solutions of C_{10}mimNTf$_2$. The corresponding phase diagrams are shown in Figures 2 and 3. Figure 2a shows the phase diagrams of the mixtures of C_8mimNTf$_2$ with the alcohols 1-octanol (C_8OH), 1-nonanol (C_9OH), 1-decanol (C_{10}OH), 1-undecanol (C_{11}OH), and 1-dodecanol (C_{12}OH); Figure 2b shows those of the mixtures with 1-tetradecanol (C_{14}OH), 1-hexadecanol (C_{16}OH), 1-octadecanol (C_{18}OH), and 1-eicosanol (C_{20}OH). The mixtures with C_{10}mimNTf$_2$, for which the phase diagrams are shown in Figure 3, include the same series of alcohols, except for 1-octanol. The curves drawn in the figures are fits using eq 3, which will be introduced and explained in the next section.

Investigations of phase diagrams for $C_x$mimNTf$_2$ + C_nOH mixtures[24−29,31] reported in the literature refer to solutions of ILs with shorter side chains in *n*-alcohols with shorter chain lengths. To our knowledge, of the mixtures studied in the present work, only the phase diagram of C_8mimNTf$_2$ in 1-octanol has been reported previously.[26] Those data are shown together with our results in Figure 4; there is perfect agreement between those data and our work. The results of the fits to our data and the data from the literature are summarized in Tables 3 and 4, respectively.

All of the investigated binary mixtures show an upper critical solution temperature (UCST). All of the curves are rather steep at small concentrations of the salt and flat at higher concentrations; in other words, the phase diagrams are rather asymmetric. The critical composition, which in binary mixtures agrees with the maximum temperature of

Table 1. Data Set for the Liquid−Liquid Phase Diagrams of C_8mimNTf$_2$ + *n*-Alkyl Alcohol Mixtures: Mass Fractions *w*, Mole Fractions x_{IL}, and Cloud-Point Temperatures T_{cloud} and Their Uncertainties δT[a]

w	x_{IL}	T_{cloud}/K	δT/K	*w*	x_{IL}	T_{cloud}/K	δT/K
			C_8mimNTf$_2$ + 1-Octanol				
0.053	0.015	293.46	0.05	0.480	0.200	308.36	0.06
0.084	0.024	300.23	0.05	0.550	0.250	307.46	0.05
0.163	0.051	306.73	0.05	0.610	0.300	305.73	0.07
0.228	0.075	308.22	0.05	0.672	0.360	302.90	0.05
0.288	0.100	308.63	0.06	0.710	0.400	300.05	0.05
0.391	0.150	309.24	0.05	0.742	0.440	297.56	0.05
0.444	0.180	308.54	0.05	0.783	0.500	291.33	0.05
			C_8mimNTf$_2$ + 1-Nonanol				
0.063	0.020	305.15	0.05	0.454	0.201	318.81	0.05
0.078	0.025	307.91	0.05	0.512	0.241	318.42	0.05
0.143	0.048	315.21	0.05	0.584	0.300	317.21	0.05
0.21	0.075	317.86	0.06	0.642	0.352	314.44	0.05
0.270	0.101	319.20	0.05	0.690	0.403	311.15	0.05
0.370	0.151	319.21	0.05	0.724	0.444	308.57	0.05
0.411	0.175	319.02	0.05	0.767	0.500	301.84	0.05
			C_8mimNTf$_2$ + 1-Decanol				
0.044	0.015	313.90	0.05	0.429	0.200	330.45	0.10
0.071	0.025	321.24	0.05	0.511	0.258	329.65	0.05
0.138	0.051	327.54	0.05	0.563	0.300	328.65	0.05
0.196	0.075	329.33	0.05	0.625	0.357	326.03	0.05
0.251	0.101	330.13	0.05	0.665	0.398	323.55	0.05
0.337	0.145	330.50	0.05	0.703	0.440	321.19	0.05
0.391	0.176	330.35	0.05	0.748	0.497	318.69	0.05
			C_8mimNTf$_2$ + 1-Undecanol				
0.040	0.015	317.26	0.05	0.408	0.200	337.33	0.05
0.066	0.025	326.87	0.50	0.472	0.245	337.19	0.10
0.127	0.050	332.62	0.20	0.543	0.301	336.04	0.10
0.182	0.075	335.05	0.05	0.600	0.352	334.57	0.10
0.233	0.099	336.31	0.20	0.653	0.406	332.05	0.10
0.282	0.125	336.77	0.10	0.691	0.448	329.15	0.10
0.326	0.149	337.19	0.10	0.731	0.496	326.72	0.05
0.329	0.151	337.12	0.05				
			C_8mimNTf$_2$ + 1-Dodecanol				
0.049	0.020	337.54	0.05	0.472	0.260	347.85	0.05
0.117	0.049	345.24	0.05	0.524	0.301	346.75	0.05
0.219	0.099	348.03	0.08	0.582	0.353	344.90	0.07
0.306	0.147	348.55	0.07	0.628	0.399	342.16	0.05
0.391	0.201	348.45	0.05	0.679	0.453	339.06	0.05
			C_8mimNTf$_2$ + 1-Tetradecanol				
0.061	0.028	351.75	0.05	0.353	0.197	364.34	0.30
0.078	0.037	357.95	0.07	0.425	0.250	363.92	0.10
0.105	0.050	359.95	0.20	0.483	0.296	363.23	0.05
0.153	0.075	363.85	0.10	0.543	0.349	361.88	0.05
0.200	0.101	364.00	0.05	0.551	0.356	361.01	0.05
0.281	0.150	364.45	0.06				
			C_8mimNTf$_2$ + 1-Hexadecanol				
0.048	0.025	366.59	0.15	0.390	0.246	379.95	0.10
0.105	0.057	375.87	0.05	0.454	0.298	379.88	0.05
0.175	0.098	379.22	0.05	0.523	0.359	378.85	0.05
0.255	0.149	379.85	0.05	0.576	0.409	374.62	0.05
			C_8mimNTf$_2$ + 1-Octadecanol				
0.051	0.029	380.65	0.15	0.383	0.261	397.85	0.05
0.080	0.047	389.03	0.15	0.429	0.299	396.28	0.10
0.156	0.095	395.57	0.10	0.483	0.347	395.25	0.10
0.239	0.152	397.06	0.05	0.541	0.402	392.88	0.14
0.276	0.178	397.2	0.05	0.592	0.452	391.42	0.08
0.337	0.224	397.81	0.05				
			C_8mimNTf$_2$ + 1-Eicosanol				
0.038	0.024	391.72	0.05	0.400	0.295	433.08	0.05
0.072	0.046	413.14	0.05	0.463	0.351	430.58	0.05
0.148	0.099	428.37	0.10	0.517	0.402	427.87	0.07
0.286	0.201	438.05	0.05	0.561	0.446	422.56	0.05
0.350	0.253	436.05	0.06				

[a] The uncertainties were determined by the accuracy of the *T* measurement and the repeatability of the T_{cloud} measurements. The uncertainty in the mole fraction is $\Delta x_{IL} = \pm 10^{-3}$ as a result of the accuracy of the weight measurements and the sample size.

the phase diagrams, is located at low concentrations, in the mole fraction range $0.1 < x_{IL} < 0.2$.

The critical temperatures increase with the chain length of the alcohols. Comparing the two ILs, we note a decrease in the critical temperature with increasing chain length of the side chain of the imidazolium cation. The observations are in agreement with the observations on solutions of ILs with shorter side chains in alcohols with smaller chain lengths.[20−22] They are also in agreement with observations on solutions of ILs with the anions BF_4^- and PF_6^-.[12,23−26]

Table 2. Data Set for the Liquid−Liquid Phase Diagrams of C_{10}mimNTf$_2$ + *n*-Alkyl Alcohol Mixtures (for Symbols and Remarks on Uncertainties, see Table 1)

w	x_{IL}	T_{cloud}/K	δT/K	w	x_{IL}	T_{cloud}/K	δT/K
			C_{10}mimNTf$_2$ + 1-Nonanol				
0.082	0.025	289.40	0.50	0.535	0.248	295.23	0.15
0.153	0.049	294.26	0.15	0.620	0.319	292.09	0.20
0.279	0.100	296.41	0.05	0.675	0.373	288.85	0.10
0.381	0.150	296.50	0.05	0.698	0.398	286.95	0.40
0.435	0.181	296.39	0.05	0.739	0.448	282.55	0.60
			C_{10}mimNTf$_2$ + 1-Decanol				
0.075	0.025	298.55	0.40	0.470	0.218	306.99	0.08
0.138	0.048	303.05	0.30	0.538	0.268	305.08	0.05
0.233	0.087	306.88	0.08	0.631	0.350	301.75	0.30
0.339	0.139	307.94	0.05	0.697	0.420	297.05	0.20
0.399	0.173	307.80	0.08				
			C_{10}mimNTf$_2$ + 1-Undecanol				
0.070	0.0251	304.34	0.11	0.509	0.2619	313.62	0.05
0.135	0.0507	310.55	0.15	0.579	0.3198	311.50	0.10
0.247	0.1008	313.42	0.05	0.630	0.3682	309.27	0.05
0.329	0.1437	313.82	0.06	0.669	0.4093	306.74	0.16
0.413	0.1938	313.98	0.08	0.715	0.4619	302.85	0.10
			C_{10}mimNTf$_2$ + 1-Dodecanol				
0.045	0.017	313.16	0.06	0.473	0.249	324.27	0.12
0.126	0.051	322.93	0.10	0.610	0.367	319.53	0.20
0.202	0.085	325.26	0.06	0.675	0.435	317.34	0.05
0.293	0.133	325.35	0.10	0.740	0.513	308.45	0.25
0.392	0.192	325.54	0.05				
			C_{10}mimNTf$_2$ + 1-Tetradecanol				
0.057	0.025	332.01	0.15	0.448	0.257	339.20	0.05
0.099	0.045	337.45	0.20	0.506	0.304	337.89	0.10
0.190	0.091	340.14	0.06	0.540	0.333	336.76	0.09
0.255	0.127	340.21	0.08	0.605	0.395	333.74	0.09
0.372	0.202	340.02	0.07	0.688	0.484	327.75	0.20
			C_{10}mimNTf$_2$ + 1-Hexadecanol				
0.067	0.033	346.55	0.20	0.408	0.249	352.13	0.07
0.108	0.055	349.84	0.15	0.460	0.291	351.15	0.06
0.225	0.123	352.68	0.05	0.511	0.335	349.67	0.05
0.262	0.146	352.77	0.05	0.543	0.364	348.27	0.07
0.271	0.152	352.79	0.05	0.585	0.404	346.36	0.10
			C_{10}mimNTf$_2$ + 1-Octadecanol				
0.045	0.025	352.35	0.60	0.389	0.255	363.00	0.05
0.089	0.050	359.85	0.20	0.458	0.312	361.78	0.08
0.155	0.090	363.01	0.08	0.478	0.330	361.05	0.10
0.231	0.139	363.45	0.10	0.483	0.334	360.90	0.15
0.313	0.197	363.54	0.05				
			C_{10}mimNTf$_2$ + 1-Eicosanol				
0.042	0.025	361.60	0.40	0.378	0.265	374.32	0.05
0.084	0.052	370.05	0.20	0.448	0.325	372.98	0.05
0.142	0.089	373.80	0.05	0.501	0.373	371.14	0.05
0.215	0.140	374.66	0.08	0.536	0.406	369.79	0.05
0.284	0.190	374.77	0.05	0.577	0.447	367.27	0.08

The observed trends correspond to the expectations based on chemical reasoning. An increase of the hydrophobicity of the IL resulting from the increase in the length of the side chain of the cation enhances the solubility in weakly polar organic solvents, which corresponds to a decrease in the separation temperature. Analogously, reducing the polarity of the solvent by increasing the chain length of the alcohol reduces the stability of the solution, causing the separation temperature to increase. The variation of the other properties of the phase diagrams with the chain length of the alcohols and the length of the side chain of the cations could not be extracted by inspection from the phase diagrams. The shapes of the curves appear very similar for all of the systems. The maxima were difficult to determine because the tops of the curves are rather flat. Therefore, a numerical analysis of the shape of the phase diagrams was carried out.

Shape Analysis of the Coexistence Curves. In order to allow for a quantitative assessment, the phase diagrams were analyzed by fitting to an analytical expression yielding the parameters characterizing the curves. The applied expression is based on scaling laws used in the field of critical phenomena.[27,32,35,36] In the analysis, we presume Ising criticality and take into account the asymmetry of the phase diagrams using the rectilinear diameter rule of Cailletet and Mathias.[36] The simplified scaling laws applied in the analysis are

$$X_{\pm} - X_m = \pm B \cdot (T_c - T)^{1/3} \quad (1)$$

where

$$X_m = X_c + A \cdot (T_c - T) \quad (2)$$

X denotes the composition variable, which in this work is the mole fraction x_{IL}; X_c is the critical composition; X_m is the diameter defined as $(X_+ + X_-)/2$, where X_+ and X_- are the compositions in the two phases; T is the system absolute

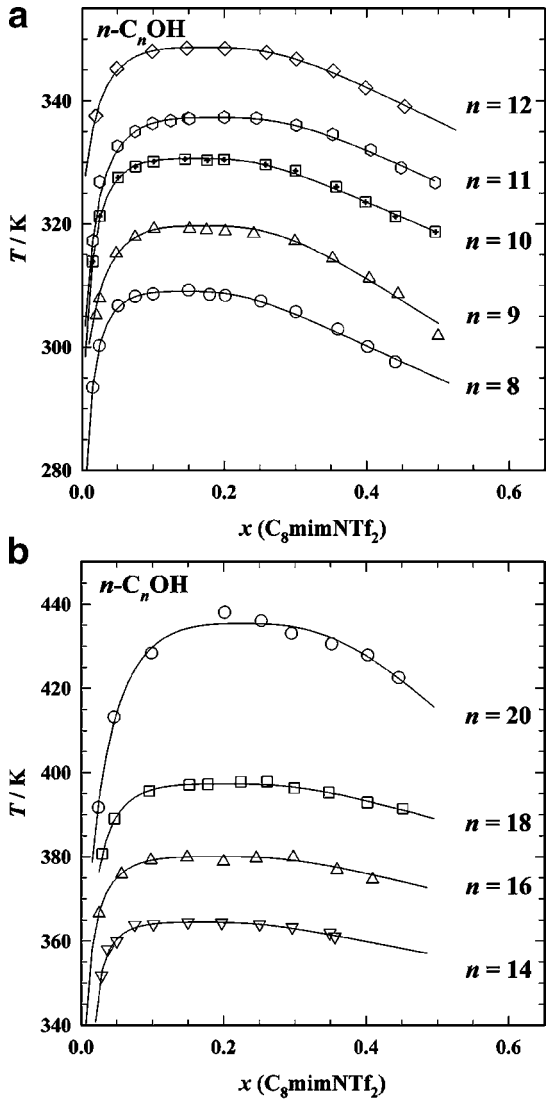

Figure 2. Isobaric phase diagrams at ambient pressure for C_8mimNTf$_2$ + n-alkyl alcohol (C_nOH) mixtures, with the mole fraction x_{IL} as the concentration variable: (a) $n = 8, 9, 10, 11, 12$; (b) $n = 14, 16, 18, 20$. The uncertainties in T and x are not visible in the resolution of the plot. The lines were calculated with the parameters shown in Table 3, which were obtained by fitting the experimental data with eq 3.

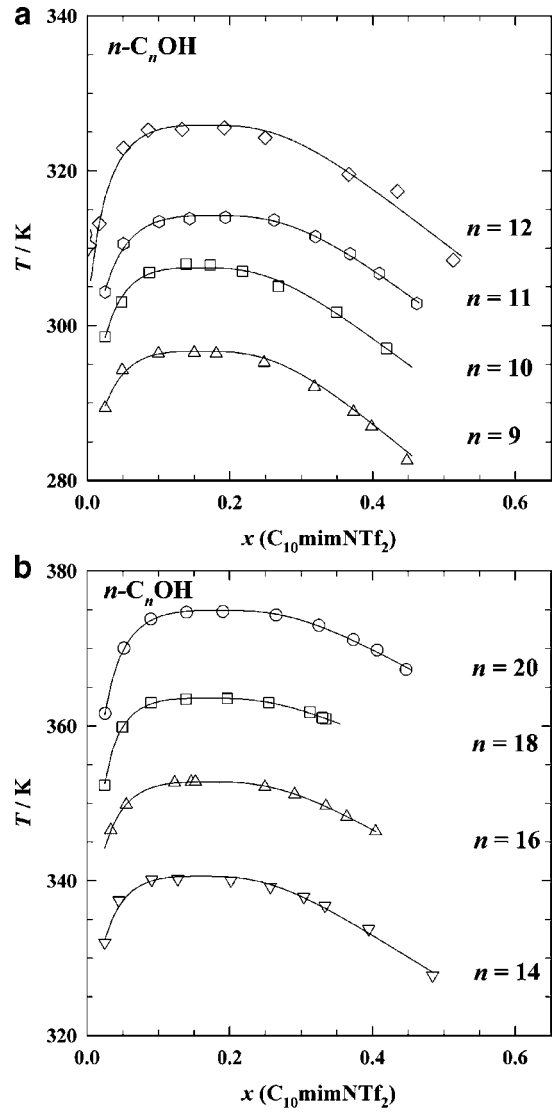

Figure 3. Isobaric phase diagrams at ambient pressure for C_{10}mimNTf$_2$ + *n*-alkyl alcohol (C_nOH) mixtures, with the mole fraction x_{IL} as the concentration variable: (a): $n = 9, 10, 11, 12$; (b): $n = 14, 16, 18, 20$. Symbols, lines, and uncertainties have the same meanings as in Figure 2.

temperature; and T_c is the critical temperature. The shape of the phase diagram is characterized by the width of the coexistence curve, B, defined in eq 1 and the parameter A defined in eq 2. It should be noted that the slope of the rectilinear diameter in the phase diagram is $-1/A$. Equations 1 and 2 lead to a cubic equation for T, which can be solved exactly. However, the resulting solutions are too complicated to be applied in a fitting procedure. In many cases, the deviation from the symmetrical shape of the phase diagram is not very large, so an expansion of $|X - X_m|^3$ to first order in A suffices. The resulting function $T(X)$, which we applied in fitting the data, is

$$T(X) = T_c - \frac{|X - X_c|^3}{B^3 \pm 3A \cdot (X - X_c)^2} \qquad (3)$$

The positive and negative signs correspond to the ranges $X < X_c$ and $X > X_c$, respectively. The parameters of the fit are the critical data, T_c and X_c, the width of the coexistence curve, B, and the slope parameter of the diameter, A. From such a fit, the nonclassical shape of the phase diagrams is taken into account to a reasonable approximation. The approximation of the critical exponent β by $\beta = 1/3$ is near the Ising β value of 0.326,[36] which suffices here. This approximation was also used by Guggenheim.[37] In mean-field theories such as the van der Waals theory or the theory of regular solutions and in all sophisticated modifications of those theories, the exponent β has the value $1/2$[36] so the equations corresponding to eqs 1 and 2 lead to a quadratic equation with a simple exact solution. It should be noted that straightforward fits by an analytic power series not only imply classical exponents, which are fundamentally wrong, but often also lead to erroneous descriptions, e.g., by showing spurious maxima.

We recall that the nature of the critical point of phase transitions of ionic solutions was a matter of discussion for some time.[38−40] The reason for this discussion was the long-range nature of the Coulomb interactions, which vary with r as r^{-1} and determine the thermodynamics of ionic solutions. However, universal Ising behavior, which is generally found for the liquid−gas and liquid−liquid transitions of nonionic systems, can only be expected when short-range interactions r^{-k} with $k > 5$ determine the phase transition. Because the Coulomb

Table 3. Parameters of the Liquid−Liquid Phase Diagrams of Solutions of Ionic Liquids with the NTf_2^- Anion Obtained by Fitting the Experimental Curves with Equation 3 Using the Mole Fraction as the Composition Variable: Critical Mole Fractions x_c, Critical Temperatures T_c, Widths of the Coexistence Curves B, and Values of the Parameter A That Determines the Slope of the Rectilinear Diameter Are Given, Along with Their Asymptotic Standard Errors Provided by the Fitting Routine and the Standard Deviations (σ) of the Fits from the Experimental Data

system	T_c/K	x_c	B/K$^{-1/3}$	A/K^{-1}	σ/K
C_8mimNTf_2 + C_8OH	309.1 ± 0.2	0.147 ± 0.005	0.080 ± 0.002	0.0066 ± 0.0004	0.94
C_8mimNTf_2 + C_9OH	319.7 ± 0.3	0.170 ± 0.005	0.085 ± 0.002	0.0051 ± 0.0004	0.75
C_8mimNTf_2 + C_{10}OH	330.7 ± 0.1	0.159 ± 0.003	0.087 ± 0.001	0.0075 ± 0.0003	0.55
C_8mimNTf_2 + C_{11}OH	337.3 ± 0.1	0.186 ± 0.002	0.095 ± 0.001	0.0070 ± 0.0003	0.91
C_8mimNTf_2 + C_{12}OH	348.7 ± 0.1	0.171 ± 0.003	0.092 ± 0.001	0.0067 ± 0.0004	0.33
C_8mimNTf_2 + C_{14}OH	364.5 ± 0.2	0.168 ± 0.006	0.096 ± 0.005	0.0115 ± 0.0019	0.17
C_8mimNTf_2 + C_{16}OH	380.0 ± 0.2	0.190 ± 0.010	0.103 ± 0.006	0.0093 ± 0.0026	0.87
C_8mimNTf_2 + C_{18}OH	397.3 ± 0.2	0.200 ± 0.003	0.100 ± 0.002	0.0081 ± 0.0006	0.41
C_8mimNTf_2 + C_{20}OH	435.3 ± 0.9	0.226 ± 0.007	0.078 ± 0.003	0.0023 ± 0.0006	1.92
C_{10}mimNTf_2 + C_9OH	296.7 ± 0.2	0.155 ± 0.004	0.082 ± 0.002	0.0050 ± 0.0004	0.44
C_{10}mimNTf_2 + C_{10}OH	307.5 ± 0.2	0.159 ± 0.006	0.083 ± 0.002	0.0056 ± 0.0007	0.31
C_{10}mimNTf_2 + C_{11}OH	314.2 ± 0.2	0.177 ± 0.004	0.091 ± 0.001	0.0055 ± 0.0004	0.39
C_{10}mimNTf_2 + C_{12}OH	325.9 ± 0.6	0.168 ± 0.013	0.086 ± 0.004	0.0053 ± 0.0010	2.53
C_{10}mimNTf_2 + C_{14}OH	340.6 ± 0.3	0.160 ± 0.006	0.087 ± 0.003	0.0066 ± 0.0005	0.54
C_{10}mimNTf_2 + C_{16}OH	352.8 ± 0.1	0.170 ± 0.001	0.093 ± 0.001	0.0073 ± 0.0002	0.05
C_{10}mimNTf_2 + C_{18}OH	363.6 ± 0.1	0.170 ± 0.001	0.096 ± 0.001	0.0098 ± 0.0005	0.1
C_{10}mimNTf_2 + C_{20}OH	374.9 ± 0.1	0.185 ± 0.003	0.096 ± 0.001	0.0076 ± 0.0004	0.27

interactions are long-range interactions, it was hypothesed that phase separation in ionic systems may show mean-field critical behavior. Such behavior has indeed been reported[41,42] but could not be confirmed in later measurements.[43] Simulations on model fluids of charged hard spheres yield Ising critical behavior;[44−46] theory excludes mean-field behavior,[47,48] and experiments on phase transitions of ionic solutions prove Ising criticality[43,49−52] or are at least consistent with Ising behavior.[12,14,32,53] Thus, it is now almost certain that the liquid−liquid phase transitions of ionic solutions belong to the Ising universality class. Other results are most likely caused by experimental shortcomings.[54] Therefore, the application of eq 3 that presumes Ising criticality is justified. This equation takes into account the nonclassical Ising nature of the phase diagrams as well as the fact that, in variance to the Ising model, the phase diagrams of fluids are in general asymmetric. A consequence of the asymmetry is that the average composition of the two phases, known as the diameter, is not constant but varies with temperature. We may mention that the linear temperature variation of the diameter presumed in eq 2 in accordance with the Cailletet−Mathias rectilinear diameter rule is only an approximation. It is now known that the diameter is a sum of a linear term and nonanalytical terms[55] that are determined by critical exponents 2β and $1 - \alpha$, where $\alpha = 0.11$ is the critical exponent of the specific heat, which diverges as the critical temperature is approached.[36] However, the various terms often cancel to some extent, so the linear approximation used in eq 2 turns out to work well in many cases.[55] The assessment of the nonanalytic terms of the diameter of the coexistence curve would require measurements with an accuracy of 10^{-3} K in the critical region, which is outside the scope of this work. Equation 3 has been proved to work reasonably well in the region up 10 K below T_c.[14,27,32,35] For measurements in a larger temperature region, so-called "corrections to scaling" in eq 1 or the application of a crossover theory are required.[56] In the present work, however, the accessible temperature range is restricted by crystallization of either the alcohols or the ILs, respectively, to (10 to 15) K below T_c. In Table 3 we summarize the results of the analysis of the phase diagrams. The table gives the critical temperature, the critical mole fraction, and the parameters describing the shape of the phase diagrams, which are the width parameter B and the parameter A that determines the slope of the diameter. The errors given are their asymptotic standard errors obtained from the fitting routine and the standard deviation of the fits from the experimental data. They are determined by the uncertainties of the measurements but also by the approximations involved in the fit model, e.g., neglect of the nonanalytical nature of the diameter[55] and the correction to scaling.[56]

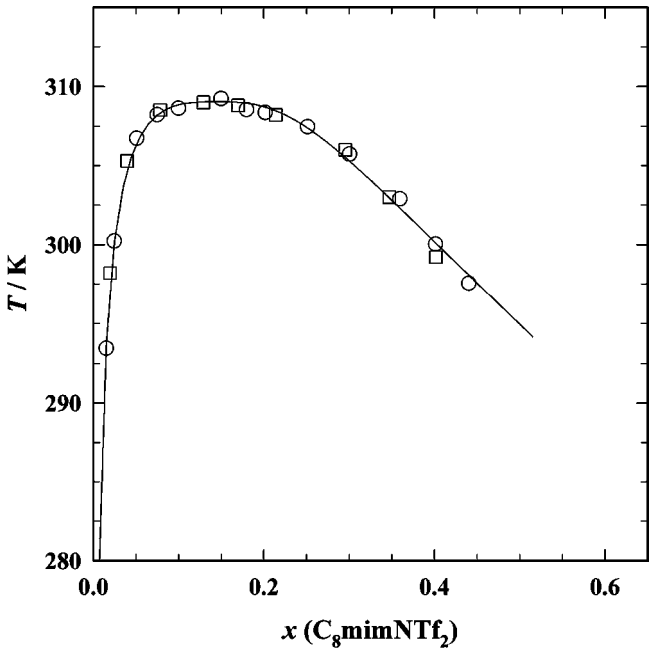

Figure 4. Direct comparison of our results (○) for the system C_8mimNTf_2 + 1-octanol with the phase diagram obtained by Crosthwaite et al. (□)[26] under similar conditions. The line indicates the results obtained by fitting our experimental data with eq 3.

For comparison and to enable a better overview of the existing systems, the results of fits of eq 3 to literature data for $C_x$mimNTf_2 + C_nOH systems are listed in Table 4. Comparing the data for x_c, B, and A in Tables 3 and 4 shows that the values are rather similar for all of these systems, although they differ in both the length of the IL side chain and the alcohol chain length.

In Figure 5a−d we summarize the contents of Tables 3 and 4 by showing the variation of the critical temperature T_c, the critical mole fraction x_c, the coexistence curve width B, and the diameter slope A as functions of the chain length of the

Table 4. Parameters of the Liquid−Liquid Phase Diagrams of Solutions of Ionic Liquids with the NTf_2^- Anion Obtained by Fitting Data Available in the Literature with Equation 3 Using the Mole Fraction as the Composition Variable; Asymptotic Standard Errors for All Quantities, Standard Deviations (σ) of the Fits from the Data, and References Are Given (Symbols Are the Same as in Table 3)

system	T_c/K	x_c	B/K$^{-1/3}$	A / K^{-1}	σ/K	ref
C_2mimNTf_2 + C_3OH	294.06 ± 0.12	0.137 ± 0.002	0.0692 ± 0.0007	0.0054 ± 0.0002	0.35	22
C_2mimNTf_2 + C_4OH	320.64 ± 0.06	0.146 ± 0.001	0.0751 ± 0.0008	0.0062 ± 0.0002	0.43	22
C_2mimNTf_2 + C_5OH	339.84 ± 0.06	0.162 ± 0.001	0.0852 ± 0.0008	0.0076 ± 0.0004	0.05	22
C_4mimNTf_2 + C_4OH	300.08 ± 0.13	0.139 ± 0.003	0.0724 ± 0.0012	0.0056 ± 0.0003	0.4	25
C_4mimNTf_2 + C_6OH	333.01 ± 0.74	0.202 ± 0.011	0.0883 ± 0.0028	0.0041 ± 0.0005	2.15	25
C_6mimNTf_2 + C_6OH	306.32 ± 0.21	0.146 ± 0.005	0.0777 ± 0.0015	0.0062 ± 0.0005	0.56	25
C_6mimNTf_2 + C_4OH	269.42 ± 0.07	0.120 ± 0.002	0.0686 ± 0.0007	0.0068 ± 0.0003	0.28	29
C_6mimNTf_2 + C_5OH	289.84 ± 0.20	0.135 ± 0.006	0.0731 ± 0.0009	0.0061 ± 0.0006	0.71	29
C_6mimNTf_2 + C_6OH	306.81 ± 0.23	0.157 ± 0.004	0.0779 ± 0.0013	0.0047 ± 0.0002	0.88	29
C_6mimNTf_2 + C_8OH	334.15 ± 0.64	0.197 ± 0.009	0.0890 ± 0.0036	0.0032 ± 0.0003	1.52	29
C_8mimNTf_2 + C_8OH	309.22 ± 0.22	0.144 ± 0.005	0.0784 ± 0.0018	0.0066 ± 0.0006	0.52	26

alcohol. In all cases, we see a trend of the parameters to increase with the chain length of the alcohol. With the exception of the critical temperatures, the variations are rather small. While the values of T_c for the C_8mimNTf_2 solutions are higher than those of the C_{10}mimNTf_2 solutions, no clear difference can be seen for the other parameters x_c, A, and B characterizing the phase diagrams. It is noticeable that for the systems C_8mimNTf_2 with long-chain alcohols C_nOH ($n \geq 18$), the T_c curve shows a significant bending toward higher temperatures in comparison with the C_{10}mimNTf_2 data.

General Discussion. In order to put our results in the context of other work where phase diagrams of mixtures containing $C_x$mimNTf_2 ILs with shorter side chains were investigated,[22,25,26,29] the critical temperatures determined for our systems are shown in Figure 6 together with those from the literature.

As the critical temperatures for mixtures with C_{10}mimNTf_2 approach the region of the melting temperatures of the pure alcohols, the latter are also included.[57] Remarkably, similar shapes are observed for the curves describing the dependence

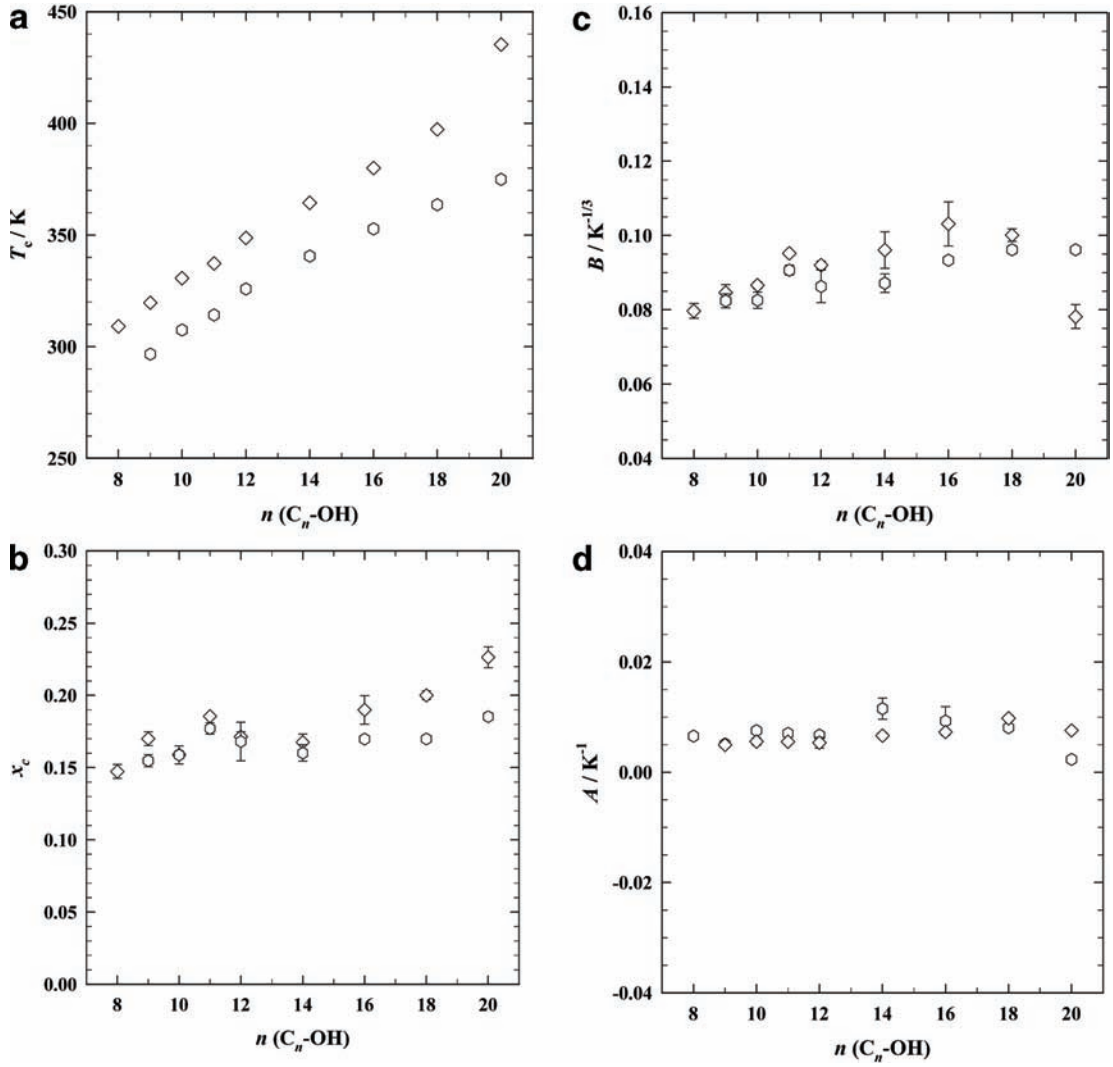

Figure 5. Representation of the characteristics of the phase diagrams for C_8mimNTf_2 (◇) and C_{10}mimNTf_2 (⬡) + C_nOH mixtures obtained by fitting with eq 3, as functions of the alcohol chain length n: (a) critical temperature T_c; (b) critical mole fraction x_c; (c) width of the coexistence region B; (d) the parameter A that determines the slope of the rectilinear diameter.

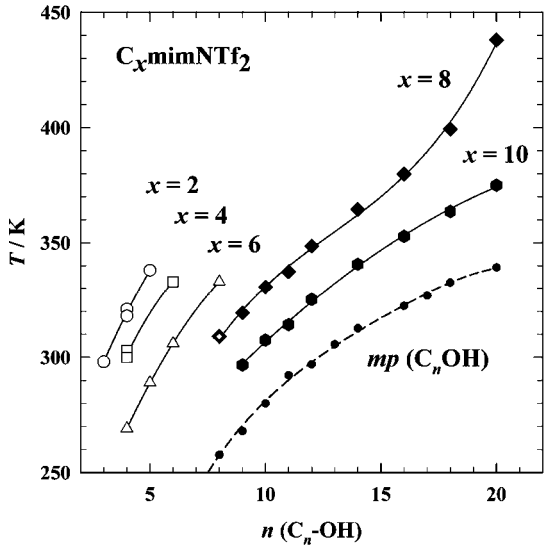

Figure 6. Dependence of the UCST on the chain length of C_nOH for different $C_x$mimNTf$_2$: solid symbols, $x = 8$, 10 (this work); open symbols, $x = 2$, 4, 6 (data from the literature[22,25,26,29]). The melting temperatures of the alcohols [labeled as *mp* (C_nOH)][57] show a chain-length dependence similar to that of the UCSTs of the investigated systems. Lines in the picture are given to illustrate trends and guide the eye.

of the critical temperatures and the alcohol melting temperatures on the length of the alcohols.

It is obvious from Figure 6 that the UCST shows a systematic increase with increasing chain length of the alcohol. Such behavior is characteristic of a small stepwise change in the interactions between solvent and solute, as mentioned above. The data obtained in this study show excellent agreement with the data set of Crosthwaite et al.[26] and fill the gap in the landscape of the phase behavior for long-chain alcohols. The trends are in agreement with chemical expectations.

A further elucidation of the critical points and the shapes of the phase diagrams by searching for correlations with other properties, such as dielectric permittivities, densities, or molecular structures, is outside the scope of this work and will be given elsewhere.

Acknowledgment

We thank A. Heintz, R. Ludwig, S. Verevkin, and H. Weingärtner for discussions and shared insight.

Literature Cited

(1) *Ionic Liquids in Synthesis*, 2nd ed.; Wasserscheid, P., Welton, T., Eds.; Wiley-VCH: Weinheim, Germany, 2008.
(2) Holbrey, J. D.; Seddon, K. R. The phase behavior of 1-alkyl-3-methylimidazolium tetrafluoroborates, ionic liquids and ionic liquid crystals. *J. Chem. Soc., Dalton Trans.* **1999**, 2133–2139.
(3) Weingärtner, H. Understanding ionic liquids at the molecular level: Facts, problems, and controversies. *Angew. Chem., Int. Ed.* **2008**, *47*, 654–670.
(4) Heintz, A. Recent developments in thermodynamics and thermophysics of non-aqueous mixtures containing ionic liquids. A review. *J. Chem. Thermodyn.* **2005**, *37*, 525–535.
(5) Rebelo, L. P. N.; Canongia Lopes, J. N.; Esperanca, J. M. S. S.; Guedes, H. J. R.; Łachwa, J.; Najdanovic-Visak, V.; Visak, Z. P. Accounting for the unique, doubly dual nature of ionic liquids from a molecular thermodynamic and modeling standpoint. *Acc. Chem. Res.* **2007**, *40*, 1114–1121.
(6) Zaitsau, D. H.; Kabo, G. J.; Strechan, A. A.; Paulechka, Y. U.; Tschersich, A.; Verevkin, S. P.; Heintz, A. Experimental vapor pressures of 1-alkyl-3-methylimidazolium bis(trifluoromethylsulfonyl)imides and a correlation scheme for estimation of vaporization enthalpies of ionic liquids. *J. Phys. Chem. A* **2006**, *110*, 7303–7306.
(7) Rebelo, L. P. N.; Canongia- Lopes, J. N.; Esperanca, J. M. S. S.; Filipe, E. On the critical temperature, normal boiling point, and vapor pressure of ionic liquids. *J. Phys. Chem. B* **2005**, *109*, 6040–6043.
(8) Zaitsau, D. H.; Paulechka, Y. U.; Kabo, G. J. The kinetics of thermal decomposition of 1-butyl-3-methylimidazolium hexafluorophosphate. *J. Phys. Chem. A* **2006**, *110*, 11602–11604.
(9) Fredlake, C. B.; Crosthwaite, J. M.; Hert, D. G.; Aki, S. N. V. K.; Brennecke, J. F. Thermophysical properties of Imidazolium-Based Ionic Liquids. *J. Chem. Eng. Data* **2004**, *49*, 954–964.
(10) Brennecke, J. F.; Maginn, E. J. Ionic liquids: Innovative fluids for chemical processing. *AIChE J.* **2001**, *47*, 2384–2389.
(11) Anthony, J. L.; Maginn, E. J.; Brennecke, J. F. Solution Thermodynamics of Imidazolium-Based Ionic Liquids and Water. *J. Phys. Chem. B* **2001**, *105*, 10942–10949.
(12) Wagner, M.; Stanga, O.; Schröer, W. Corresponding states analysis of the critical points in binary solutions of room temperature ionic liquids. *Phys. Chem. Chem. Phys.* **2003**, *5*, 3943–3950.
(13) Cerdeirina, C. A.; Troncoso, I.; Ramos, C. P.; Romani, L.; Najdanovic-Visak, V.; Guedes, H. J. R.; Esperanca, J. M. S. S.; Visak, Z. P.; da Ponte, M. N.; Rebelo, L. P. N. Criticality of the [C_4mim][BF_4] + Water System. *ACS Symp. Ser.* **2005**, *901*, 175–186.
(14) Saracsan, D.; Rybarsch, C.; Schröer, W. Phase separation in solutions of room temperature ionic liquids in hydrocarbons. *Z. Phys. Chem.* **2006**, *220*, 1417–1437.
(15) Lachwa, J.; Szydlowski, J.; Makowska, A.; Seddon, K. R.; Esperanca, J. M. S. S.; Guedes, H. J. R.; Rebelo, L. P. N. Changing from an unusual high-temperature demixing to a UCST-type in mixtures of 1-alkyl-3-methylimidazolium bis{(trifluoromethyl)sulfonyl}amide and arenes. *Green Chem.* **2006**, *8*, 262–267.
(16) Domanska, U.; Casas, L. M. Solubility of phosphonium ionic liquid in alcohols, benzene, and alkylbenzenes. *J. Phys. Chem. B* **2007**, *111*, 4109–4115.
(17) Domanska, U.; Paduszynski, K. Phase equilibria study in binary systems (tetra-*n*-butylphosphonium tosylate ionic liquid + 1-alcohol, or benzene, or *n*-alkylbenzene). *J. Phys. Chem. B* **2008**, *112*, 11054–11059.
(18) *Ionic Liquids: Industrial Applications for Green Chemistry*; Rogers, R. D., Seddon, K. R., Eds.; ACS Symposium Series 818; American Chemical Society: Washington, DC, 2002.
(19) *Ionic Liquids as Green Solvents: Progress and Prospects*; Rogers, R. D., Seddon, K. R., Eds.; ACS Symposium Series 856; American Chemical Society: Washington, DC, 2003.
(20) Heintz, A.; Lehmann, J.; Wertz, C.; Jacquemin, J. Thermodynamic properties of mixtures containing ionic liquids. 4. LLE of binary mixtures of [C_2MIM][NTf_2] with propan-1-ol, butan-1-ol, and pentan-1-ol and [C_4MIM][NTf_2] with cyclohexanol and 1,2-hexanediol including studies of the influence of small amounts of water. *J. Chem. Eng. Data* **2005**, *50*, 956–960.
(21) Wertz, Ch.; Tschersich, A.; Lehmann, J. K.; Heintz, A. Liquid−liquid equilibria and liquid−liquid interfacial tension measurements of mixtures containing ionic liquids. *J. Mol. Liq.* **2007**, *131*−*132*, 2–6.
(22) Heintz, A.; Lehmann, J.; Wertz, C. Thermodynamic properties of mixtures containing ionic liquids. 3. Liquid−liquid equilibria of binary mixtures of 1-ethyl-3-methylimidazolium bis(trifluoromethylsulfonyl)imide with propan-1-ol, butan-1-ol, and pentan-1-ol. *J. Chem. Eng. Data* **2003**, *48*, 472–474.
(23) Wu, C. T.; Marsh, K. N.; Deev, A. V.; Boxall, J. A. Liquid−liquid equilibria of room-temperature ionic liquids and butan-1-ol. *J. Chem. Eng. Data* **2003**, *48*, 486–491.
(24) Marsh, K. N.; Deev, A.; Wu, C. T.; Tran, E.; Klamt, A. K. Room temperature ionic liquids as replacements for conventional solvents - A review. *Korean J. Chem. Eng.* **2002**, *19*, 357–362.
(25) Crosthwaite, J. M.; Aki, S. N. V. K.; Maginn, E. J.; Brennecke, J. F. Liquid phase behavior of imidazolium-based ionic liquids with alcohols. *J. Phys. Chem. B* **2004**, *108*, 5113–5119.
(26) Crosthwaite, J. M.; Aki, S. N. V. K.; Maginn, E. J.; Brennecke, J. F. Liquid phase behavior of imidazolium-based ionic liquids with alcohols: effect of hydrogen bonding and non-polar interactions. *Fluid Phase Equilib.* **2005**, *228*−*229*, 303–309.
(27) Butka, A.; Vale, V. R.; Saracsan, D.; Rybarsch, C.; Weiss, V. C.; Schröer, W. The Liquid−Liquid Phase Transition in Solutions of Ionic Liquids with Halide Anions: Criticality and Corresponding States. *Pure Appl. Chem.* **2008**, *80*, 1613–1630.
(28) Sahandzhieva, K.; Tuma, D.; Breyer, S.; Kamps, A.; Maurer, G. Liquid−liquid equilibrium in mixtures of the ionic liquid 1-*n*-butyl-3-methylimidazolium hexafluorophosphate and an alkanol. *J. Chem. Eng. Data* **2006**, *51*, 1516–1525.
(29) Lachwa, J.; Morgado, P.; Esperanca, J. M. S. S.; Guedes, H. J. R.; Canongia Lopes, J. N.; Rebelo, L. P. N. Fluid-Phase Behavior of {1-Hexyl-3-methylimidazolium Bis(trifluoromethylsulfonyl) Imide, [C_6mim][NTf_2], + C_2−C_8 *n*-Alcohol} Mixtures: Liquid−Liquid Equilibrium and Excess Volumes. *J. Chem. Eng. Data* **2006**, *51*, 2215–2221.

(30) Lachwa, J.; Szydlowski, J.; Najdanovic-Visak, V.; Rebelo, L. P. N.; Seddon, K. R.; da Ponte, M. N.; Esperanca, J. M. S. S.; Guedes, H. J. R. Evidence for Lower Critical Solution Behavior in Ionic Liquid Solutions. *J. Am. Chem. Soc.* **2005**, *127*, 6542–6543.
(31) Ferreira, R.; Blesic, M.; Trindade, J.; Marrucho, I.; Canongia-Lopes, J. N.; Rebelo, L. P. N. Solubility of fluorinated compounds in a range of ionic liquids. Cloud-point temperature dependence on composition and pressure. *Green Chem.* **2008**, *10*, 918–928.
(32) Schröer, W.; Vale, V. R. Liquid−liquid phase separation in solutions of ionic liquids: phase diagrams, corresponding state analysis and comparison with simulations of the primitive model. *J. Phys.: Condens. Matter.* **2009**, *21*, 424119.
(33) Swatloski, R. P.; Holbrey, J. D.; Rogers, R. D. Ionic liquids are not always green: hydrolysis of 1-butyl-3-methylimidazolium hexafluorophosphate. *Green Chem.* **2003**, *5*, 361–363.
(34) Triolo, A.; Russina, O.; Bleif, H.-J.; Di Cola, E. Nanoscale Segregation in Room Temperature Ionic Liquids. *J. Phys. Chem. B* **2007**, *111*, 4641–4644.
(35) Schröer, W. Universality and corresponding state behaviour in the phase diagrams of alcohol solutions of ionic liquids with the BF_4^- anion. *J. Mol. Liq.* **2006**, *125*, 164–173.
(36) Anisimov, M. A. *Critical Phenomena in Liquids and Liquid Crystals*; Gordon and Breach: Philadelphia, 1991.
(37) Guggenheim, E. A. The Principle of Corresponding States. *J. Chem. Phys.* **1945**, *13*, 253–261.
(38) Pitzer, K. S. Critical Phenomena in Ionic Fluids. *Acc. Chem. Res.* **1990**, *23*, 333–338.
(39) Fisher, M. E. The Story of Coulombic Criticality. *J. Stat. Phys.* **1994**, *75*, 1–36.
(40) Weingärtner, H.; Schröer, W. Criticality of Ionic Fluids. *Adv. Chem. Phys.* **2001**, *116*, 1–66.
(41) Singh, R. R.; Pitzer, K. S. Near-Critical Coexistence Curve and Critical Exponent of an Ionic Fluid. *J. Chem. Phys.* **1990**, *92*, 6775–6778.
(42) Zhang, K. C.; Briggs, M. E.; Gammon, R. W.; Levelt Sengers, J. M. H. The susceptibility critical exponent for a nonaqueous ionic binary mixture near a consolute point. *J. Chem. Phys.* **1992**, *97*, 8692–8697.
(43) Wiegand, S.; Briggs, M. E.; Levelt Sengers, J. M. H.; Kleemeier, M.; Schröer, W. Turbidity, light scattering, and coexistence curve data for the ionic binary mixture triethyl-*n*-hexylammonium triethyl-*n*-hexylborate in diphenyl ether. *J. Chem. Phys.* **1998**, *109*, 9038–9051.
(44) Caillol, J. M.; Levesque, D.; Weiss, J. J. Critical behavior of the restricted primitive model revisited. *J. Chem. Phys.* **2002**, *116*, 10794–10800.
(45) Orkoulas, G.; Panagiotopoulos, A. Z. Phase behavior of the restricted primitive model and square-well fluids from Monte Carlo simulations in the grand canonical ensemble. *J. Chem. Phys.* **1999**, *110*, 1581–1590.
(46) Yan, Q. L.; de Pablo, J. J. Hyper-parallel tempering Monte Carlo: Application to the Lennard-Jones fluid and the restricted primitive model. *J. Chem. Phys.* **1999**, *111*, 9509–9515.
(47) Lee, B. P.; Fisher, M. E. Ginzburg criterion for Coulombic criticality. *Phys. Rev. Lett.* **1996**, *77*, 3561–3564.
(48) Schröer, W.; Weiss, V. C. Ginzburg criterion for the crossover behavior of model fluids. *J. Chem. Phys.* **1998**, *109*, 8504–8513.
(49) Kleemeier, M.; Wiegand, S.; Schröer, W.; Weingärtner, H. The liquid−liquid phase transition in ionic solution: Coexistence curves of tetra-*n*-butylammonium picrate in alkylalcohols. *J. Chem. Phys.* **1999**, *110*, 3085–3099.
(50) Oleinikova, A.; Bonetti, M. Coexistence curve of the ionic binary mixture tetra-*n*-butylammonium picrate in 1-dodecanol. *Chem. Phys. Lett.* **1999**, *299*, 417–422.
(51) Wagner, M.; Stanga, O.; Schröer, W. The liquid−liquid coexistence of binary mixtures of the room temperature ionic liquid 1-methyl-3-hexylimidazolium tetrafluoroborate with alcohols. *Phys. Chem. Chem. Phys.* **2004**, *6*, 4421–4431.
(52) Schröer, W.; Wiegand, S.; Weingärtner, H. The effect of short-range hydrogen-bonded interactions on the nature of the critical point of ionic fluids. Part II: Static and dynamic light scattering on solutions of ethylammonium nitrate in *n*-octanol. *Ber. Bunsen.-Ges. Phys. Chem.* **1993**, *97*, 975–982.
(53) Barthel, J.; Carl, E.; Gores, H. J. Coulombic liquid−liquid phase separation of dilithium hexafluoropropane-1,3-bis[sulfonylbis(trifluoromethylsulfonyl)methanide] solutions in diethylcarbonate. *Electrochem. Solid State Lett.* **1999**, *2*, 218–221.
(54) Schröer, W.; Wagner, M.; Stanga, O. Apparent Mean-Field Criticality of Liquid−Liquid Phase Transitions in Ionic Solutions. *J. Mol. Liq.* **2006**, *127*, 2–9.
(55) Wang, J.; Cenderina, C. A.; Anisimov, M. A.; Sengers, J. V. Principle of isomorphism and complete scaling for binary-fluid criticality. *Phys. Rev. E* **2008**, *77*, 031127.
(56) Gutkowski, K.; Anisimov, M. A.; Sengers, J. V. Crossover criticality in ionic solutions. *J. Chem. Phys.* **2001**, *114*, 3133–3148.
(57) *Handbook of Chemistry and Physics*, 76th ed.; Lide, D. R., Ed.; CRC Press: Boca Raton, FL, 1995.

Received for review November 20, 2009. Accepted February 25, 2010. This work was supported by the German Research Foundation (DFG) within the Priority Program SPP-1191 “Ionic Liquids” (Grant RA 1054/2-1 and SCHR 188/10-1).

JE900988A